Journal of Nanoscience and Nanotechnology
Vol. 11, 6007–6012, 2011

Hydrothermal Synthesis of Anatase TiO_2 Nanorods with High Crystallinity Using Ammonia Solution as a Solvent

Dong Ri Zhang[2], Hyun Gil Cha[1], and Young Soo Kang[1,*]

[1] *Department of Chemistry, Sogang University, #1 Shinsu-dong, Mapo-gu, Seoul 121-742, Korea*
[2] *Department of Chemical Engineering and Polymer Science, College of Engineering, Yanbian University, Yanji 133002, China*

Anatase TiO_2 nanorods with high crystallinity were synthesized using ammonia solution (28%) as a solvent by through the hydrothermal method. The X-ray diffraction pattern confirmed the product's anatase phase and high crystallinity, and the transmission electron microscope (TEM) image demonstrated the unique morphologies of the two ends of the TiO_2 nanorods (two tringle-horn shapes and one round-horn shape), whose lengths and widths were within the ranges of 200–300 and 60–110 nm, respectively. The high-resolution TEM image clearly displayed the crystal lattices of the (101) planes lying along the direction of the lengthes of the TiO_2 nanorods. The energy dispersive X-ray spectrum of a TiO_2 nanorod revealed the presence of about 4 atm% nitrogen element as a trace in the anatase TiO_2 nanorod. The Raman spectrum of the TiO_2 nanorods also showed the typical bands of anatase TiO_2 and very weak peaks resulting from the TiN first-order defect-induced Raman scattering. The UV-vis diffuse-reflectance spectra showed a slight red shift (about 3 nm) of the anatase TiO_2 nanorods compared with P25, which probably resulted from the trace of TiN on the surfaces of the anatase TiO_2 nanorods. A three-stage-process mechanism model is proposed for the formation of the nanorods: Rhombus crystallites bounded by four {101} faces are first formed through anisotropic growth, then longer rhombus crystallites are grown via oriented attachment, finally, nanorods with a unique morphology are self-assembled by Van Der Waals forces.

Keywords: Anatase, TiO_2, Nanorod, Hydrothermal, Ammonia.

1. INTRODUCTION

One-dimensional (1D) TiO_2 nanostructures (nanorods, nanotubes, and nanowires) have received extensive attention[1–17] because their unique morphologies have several important features that depend on both their sizes and shapes. These 1D TiO_2 nanostructures are produced through a variety of methods, including the surfactant-assisted method,[1–3] the template assisted method,[4,5] hydrothermal synthesis,[6,7] solvothermal synthesis,[8] the electrochemical method,[9–12] the freeze-drying method,[13] and other methods.[14] The preparation of nanocrystalline anatase TiO_2 with the desired shapes is of great importance for the existing or potential technological applications such as photocatalysis,[2,18] solar-energy conversion,[19] sensors,[20] Li-ion batteries,[7,21] and photovoltaic devices.[22–24] TiO_2 has many advantages, such as photocatalysis efficiency, low cost, chemical inertness, and photostability, it mainly appears in three crystalline polymorphic phases: anatase, rutile, and brookite. Among these phases, anatase TiO_2 exhibits the highest photocatalytic activity, making it the most effective and widely used photocatalyst. The photoactivity of TiO_2 is strongly dependent on its crystalline structure, on the crystallite size, and on the synthesis method used.[25] The optimal crystallite size was reported to be in the range of 8–10 nm for spherical nanoparticles. The smaller crystallites favor surface recombination, and the larger crystallites exhibit lower efficiencies.[26] For nanorods, the surface-to-volume ratio is higher than that found in nanospheres, which a high density of active sites available for surface reaction as well as a high interfacial charge carrier transfer rate. Morever, it is expected to reduce the electron–hole recombination rate through the increased delocalization of the charge carrier moving freely throughout the length of the crystal.

*Author to whom correspondence should be addressed.

1533-4880/2011/11/6007/006
doi:10.1166/jnn.2011.4323

It seems that concentrated base solvents are essential for the fabrication of 1D TiO_2 nanomaterials using the hydrothermal method. Kasuga et al.[27] first reported the synthesis of a TiO_2 nanotube using 10 M NaOH solution as a solvent, through the hydrothermal method. After the report, many research groups[28–33] synthesized TiO_2-based nanotubes using the same methods. They all used 10 M NaOH or KOH aqueous solutions as solvents and obtained similar results. Sodium or potassium titanate nanotubes, however, were often obtained instead of pure TiO_2 nanotubes owing to the difficulty of completely removing Na or K ions from the products. There have been a number of reports[1–4, 6–8, 14] regarding the synthesizing of anatase TiO_2 nanorods. Here a new approach for the synthesis of anatase TiO_2 nanorods with high crystallinity is proposed for the first time, using ammonia solution as a solvent instead of alkaline metal hydroxide solutions, which are well known that the base plays a key role in the synthesis of 1D TiO_2 nanostructures. Ammonia solution is also a well-known strong base, and it is expected that 1D TiO_2 nanostructures will be obtained if ammonia solution will be used as the solvent. As expected, the synthesized products were confirmed to be anatase TiO_2 nanorods with high crystallinity. A three-stage-process mechanism model was proposed for the synthesized TiO_2 nanords with unique morphologies.

2. EXPERIMENTAL DETAILS

2.1. Synthesis of Anatase TiO_2 Nanorods

In a typical synthesis, 1.5 mL titanium butoxide ($Ti(O(CH_2)_3CH_3)_4$, 97+%, Aldrich) was mixed with 30 mL ammonia solution (NH_3, 28%, Junsei) in a Teflon container, after which the container was moved into an autoclave and was heated in a furnace at 180 °C for 38 h. After cooling to room temperature, the final precipitate was filtered and washed several times with de-ionized water and absolute ethyl alcohol (C_2H_5OH, 99.9%, Hayman), respectively. The product was then freely dried at room temperature. The synthesis procedure was repeated several times, and reproducible results were obtained.

2.2. Characterization

The crystal structure of the synthesized products were identified using powder X-ray diffraction (XRD) with a Philips X'Pert-MPD system with a Cu Kα radiation source (λ = 0.154056 nm). The size and shape of the products were determined based on transmission electron microscopy (TEM) images. TEM samples were prepared on a corbon-coated 400-mesh copper grid. TEM measurements were carried out on a HITACHI H-7500 (low-resolution) and a JEOL JEM2010 (high-resolution) transmission electron microscope (TEM). Energy-dispersive X-ray (EDX) spectroscopy for the elemental analysis and the selected-area electron diffraction (SAED) pattern of the sample was conducted on a JEOL JEM2010 TEM operated under an acceleration voltage of 200 kV. The UV-visible diffuse-reflectance spectra were measured using a Cary 3 spectrophotometer (Varian). The Raman spectra were recorded on a FRA 106/S Raman spectrometer (Bruker, Germany), and Nd/YAG laser (1064 nm) was used as an exciting light source.

3. RESULTS AND DISCUSSION

Figure 1 shows the XRD pattern of the product. The discernible peaks can be indexed to the (101), (103), (004), (112), (200), (105), (211), (204), (116), (220) and (215) planes of a tetragonal unit cell, which correspond to those of the titanium dioxide structure (JCPDS card no. 83-2243). The product was determined to be in the pure anatase phase. It can be easily seen in the XRD pattern that the diffraction intensity and shape of the (101) peak are very strong and narrow, and that all the characteristic peaks pertaining to the anatase phase are clearly separated, which are different from the previous reports,[1–4] indicating that almost all the products are anatase-phase TiO_2 with very high crystallinity. This is further confirmed by the high-resolution TEM (HRTEM) images below. Cozzoli et al.[1] synthesized anatase TiO_2 nanorods using the surfactant-assisted method, at a low temperature (80 °C). The XRD profile of the TiO_2 sample clearly exhibited an extreme peak intensity and a narrow width for the (004) reflex and a comparatively lower diffraction intensity for the (200) reflex, supporting the preferential growth of TiO_2 along the [001] direction. Jun et al.[3] reported similar XRD patterns of a higher-intensity (004) peak compared to the (200) peak. In the present study, however, the intensity of the (200) peak is slightly larger than that of the (004) peak in the XRD pattern. Therefore, no information supporting the preferential growth of TiO_2 along any direction can be found in the XRD pattern.

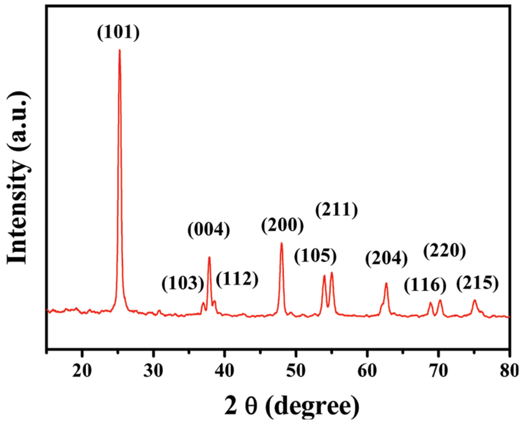

Fig. 1. XRD pattern of the anatase TiO_2 nanorods.

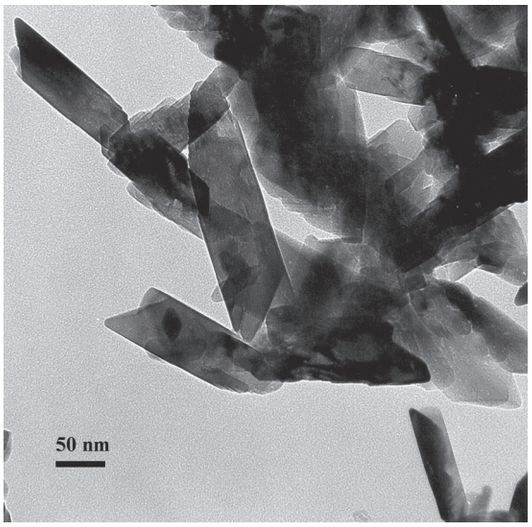

Fig. 2. TEM image of the anatase TiO_2 nanorod.

Figure 2 clearly shows the TEM image of the TiO_2 nanorods. Interestingly, the two ends of the TiO_2 nanorods show different shapes: one shows two triangle-horn shapes (one big, one small) and another shows a nearly round-horn shape. Such unique morphologies of the two ends of the TiO_2 nanorods can also be seen in the other TEM images. Based on the TEM images, the lengths of the four individual TiO_2 nanorods were 138, 185, 188, and 266 nm, respectively, their widths of were 32, 48, 57, and 67 nm, respectively, and their aspect ratios were 4.3, 3.8, 3.3, and 4.0. There was almost no change in the width of any of the TiO_2 nanorods along the length direction, except for the zone near the nanorod with round-horn-shaped ends, and the edges of the TiO_2 nanorods were shown to be very sharp. The scanning electron microscopy (SEM) image of the product (not shown) shows in a large scale the morphologies of many of the TiO_2 nanorods, whose lengths and widths were within the ranges of 200–300 and 60–110 nm, respectively.

An HRTEM image of a nearly-round-horn-shaped end of an anatase TiO_2 nanorod is shown in Figure 3. Crystal lattices can be very clearly seen on the entire surface area of the TiO_2 nanorod. The observed lattice distance of the TiO_2 nanorod was 3.3 Å, which is close to the *d*-spacing of the (101) peak ($d = 3.5$ Å) in the XRD pattern. Similar values can be found in these author's previous work[34] and in other reports.[1] It can be clearly seen in Figure 3 that the (101) planes of the anatase TiO_2 nanorod are parallel to the length direction of the TiO_2 nanorod, which is different from other reports.[1–4] This is why the information supporting the preferential growth of the TiO_2 nanorod along any direction can not be found in the XRD pattern mentioned above. The inset in Figure 3 shows the SAED pattern along a (010) zone axis from the nanorod. The pattern demonstrates that the anatase nanorods are single-crystalline. A similar SAED pattern can be found in the report.[35] A much larger HRTEM image (not shown) of the two triangle-horn shapes of the ends of an anatase TiO_2 nanorod also shows very clear crystal lattices of the (101) planes, where the growth direction of the TiO_2 nanorod is also parallel to those of the (101) planes. It can be easily seen in the XRD pattern and in the HRTEM image that the grown TiO_2 nanorods were in the single-crystalline anatase phase and had high crystallinity and predominant (101) faces.

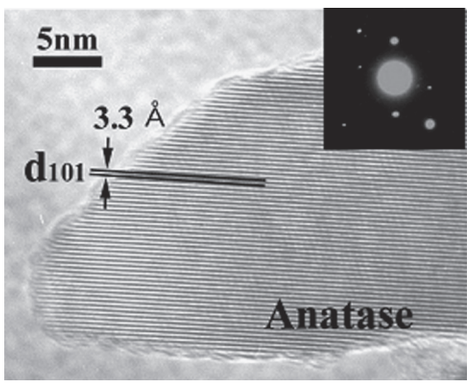

Fig. 3. HRTEM image of an anatase TiO_2 nanorod.

The unique morphologies of the ends of the nanorods triggered these authors' interest in the formation mechanism of nanorods, an explanation of which is given herein. It is proposed that there are three stages in the growth of nanorods: (1) the formation of rhombus single primary crystallites; (2) two or three (or more) rhombus single primary crystallites joining into larger single crystals via oriented attachment; and (3) the self-assembling of the larger single crystals via Van Der Waals forces.

A schematic diagram of the formation mechanism of nanorods is shown in Figure 4. In the first stage, fast hydrolysis, which is required for anisotropic crystal growth,[1] occurred after the addition of $Ti(OBu)_4$ to the NH_3 solution, as indicated by the appearance of a white cloud in the reaction solution. In this process, the reaction is kinetically driven by an extremely high monomer concentration in the early growth stages. The role of NH_3 is probably the promotion of fast crystallization in the hydrothermal conditions,[1] leading to the faster anisotropic growth of the TiO_2 crystal structure. For anatase TiO_2, the surface energy of the (001) faces is approximately

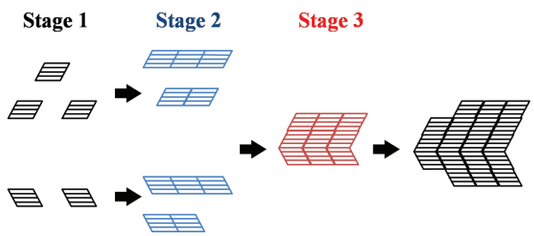

Fig. 4. Schematic diagram of the formation mechanism of nanorods.

1.4 times that of the (101) faces.[36] Thus, the initial crystal morphology will be determined by the slowest-growing faces due to the shrinking of the fastest-growing faces. Therefore, the anisotropic alloy grown monomers of the Ti-O-Ti networks further transform into small rhombus crystallites bounded by four (101) faces, and the amorphous TiO_2 nanorods are almost consumed in this stage, which was indirectly confirmed by the XRD pattern (stage 1 in Fig. 4.). These crystallites can be seen as building blocks for further particle growth. In the second stage, two (or more) small rhombus crystallites grow into larger single crystals via oriented attachment, forming longer rhombus crystallites that can be seen as small nanorods (stage 2 in Fig. 4.). Similar results can be found in the related literatures.[3, 37] This stage involves particle growth by joining small rhombus crystallites at specific dimensionally similar crystallographic surfaces. The Brownian motion of the small rhombus crystallites in the solution plays an important role in this stage. In the third and last stage, these larger single crystals begin to further grow into final products by self-assembling via Van Der Waals forces while stage 2 continues to progress (stage 3 in Fig. 4.). In this stage, the particle growth is mainly governed thermodynamically to lower the overall surface energy. It can be easily seen in the mechanism that there will be other types of nanorod morphologies in the products, as can be seen in the other TEM images (not shown).

Figure 5 shows the UV-vis diffuse-reflectance absorption spectra of the anatase TiO_2 nanorods and P25, for comparison. Both the anatase TiO_2 nanorods and P25 show the typical characteristics of anatase TiO_2,[38] with a slightly red shift (about 3 nm) of the TiO_2 nanorods compared to the P25, which rose sharply at ~380 nm. It was reported that the UV-vis absorption spectrum can also depend significantly on the nanomaterial synthesis method that is used, and on the surface environment.[5] As a result, the intepretation of the origin of the red shift is not straightforward. Such red shift has been attributed to the quantum

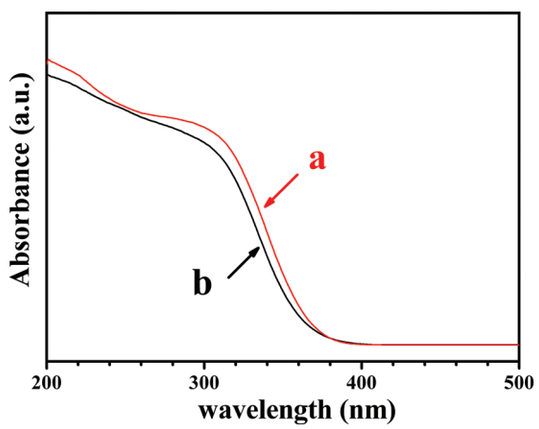

Fig. 5. UV-visible diffusereflectance spectra: (a) anatase TiO_2 nanorods and (b) TiO_2 (P25).

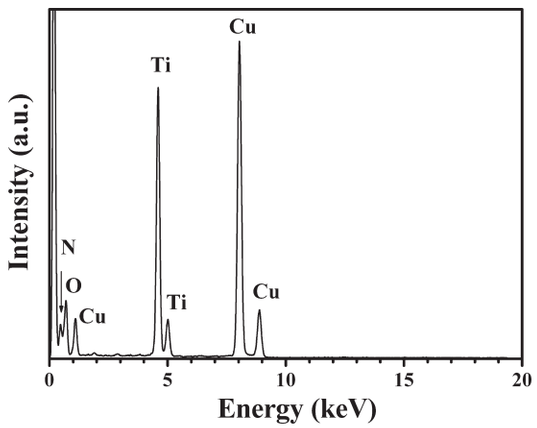

Fig. 6. Energy-dispersive X-ray spectrum of an anatase TiO_2 nanorod.

confinement effect of the crystal size in the nanometer scale.[39, 40] Martin et al.[41] observed this type of red shift for pure TiO_2 with increasing particle sizes. Hoffmann et al.[42] used a molecular orbital (MO) description to explain the optical properties of semiconductor particles during their growth from molecular to bulk sizes and the red shift was considered to correspond to a decrease in the band gap energy during the transition from quantum-to bulk-sized particles. For TiO_2 with larger than 10 nm particle sizes, however, such red shift resulting from a decrease in the band gap energy was reported to be undetectable.[42, 43] P25 (Degussa, Germany) is a well-known commercial TiO_2 photocatalyst in the anatase (80 atm%) and rutile (20 atm%) phases, and with mean crystallite sizes of ~30 nm. Thus, although the crystallite size of synthesized TiO_2 nanorods is larger than that of P25, such difference can not be considered as the reason for the red shift shown in the UV-vis diffuse-reflectance spectra of the TiO_2 nanorods compared to P25. The EDX spectrum of the TiO_2 nanorod in Figure 6 reveals the presence of about 4 atm% nitrogen as a trace in the anatase TiO_2 nanorod. The Raman spectrum of the TiO_2 nanorods in

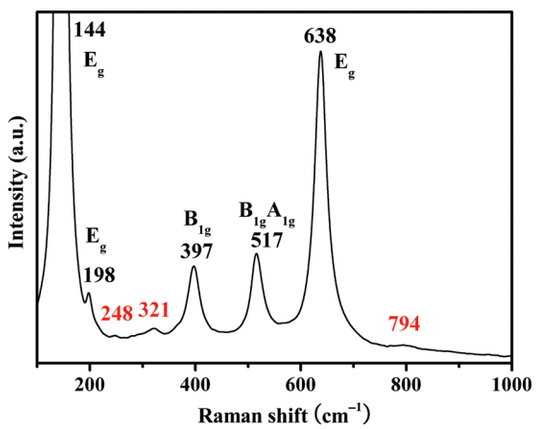

Fig. 7. Raman spectrum of the anatase TiO_2 nanorods.

Figure 7 displays the typical bands of anatase TiO_2 at 144, 198, 397, 517, and 638 cm^{-1},[7] and the very weak peaks at 248, 321, and 794 cm^{-1} resulting from TiN first-order defect-induced Raman scattering.[44] It is well-known that the Raman technique is a very sensitive tool, and is thus widely used in the field of nanomaterials. The very weak intensities from TiN further support the amount of nitrogen element (as low as 4 atm%) obtained via EDX measurement. The existence of a small amount of TiN on the surfaces of the anatase TiO_2 nanorods may be one of the reasons for the red shift as a factor of the surface environment.

4. CONCLUSIONS

In summary, a simple new approach for synthesizing anatase TiO_2 nanorods with high crystallinity using ammonia solution (28%) as a solvent, using the hydrothermal method, was demonstrated. The XRD pattern confirmed the anatase phase of the product, and the TEM image showed the unique morphologies of the two triangle- and round-horn-shaped ends of the TiO_2 nanorods. The HRTEM image clearly displayed the crystal lattices of the (101) planes lying along the direction of the length of the TiO_2 nanorod. The UV-vis diffuse-reflectance spectra showed a slight red shift (about 3 nm) of the anatase TiO_2 nanorods compared with P25, which probably resulted from the trace of TiN on the surfaces of the anatase TiO_2 nanorods. The synthesized nanorods were formed in a three stage process: (1) rhombus crystallites bounded by four (101) faces were formed through anisotropic growth; (2) longer rhombus crystallites were grown via oriented attachment,; and (3) the final nanorods were self-assembled by Van Der Waals forces. The study results modify the previously investigated hydroxide synthesis routes. The factors influencing the formation of nanorods are currently under investigation, and the elucidation of the formation mechanism of nanorods is under way.

Acknowledgments: This work was supported by the Korea Center for Artificial Photosynthesis (KCAP) located in Sogang University through the National Research Foundation of Korea (NRF-2009-C1AAA001-2009-0093879) and the Center for Next Generation Dye-sensitized Solar Cells (No. 2010-0001842) funded by the Ministry of Education, Science, and Technology (MEST) of Korea.

References and Notes

1. P. D. Cozzoli, A. Kornowski, and H. H. Weller, *J. Am. Chem. Soc.* 125, 14539 (**2003**).
2. J. Joo, S. G. Kwon, T. Yu, M. Cho, J. Lee, J. Yoon, and T. Hyeon, *J. Phys. Chem. B* 109, 15297 (**2005**).
3. Y. W. Jun, M. F. Casula, J. H. Sim, S. Y. Kim, J. Cheon, and A. P. Alivisatos, *J. Am. Chem. Soc.* 125, 15981 (**2003**).
4. J. J. Wu and C. C. Yu, *J. Phys. Chem. B* 108, 3377 (**2004**).
5. M. S. Sander, M. J. Cote, W. Gu, B. M. Kile, and C. P. Tripp, *Adv. Mater.* 16, 2052 (**2004**).
6. X. J. Feng, J. Zhai, and L. Jiang, *Angew. Chem. Int. Ed.* 44, 5115 (**2005**).
7. X. Gao, H. Zhu, G. Pan, S. Ye, Y. Lan, W. F. Feng, and D. Song, *J. Phys. Chem. B* 108, 2868 (**2004**).
8. X. L. Li, Q. Peng, J. X. Yi, X. Wang, and Y. D. Li, *Chem. Eur. J.* 12, 2383 (**2006**).
9. J. M. Macák, H. Tsuchiya, and P. Patrik Schmuki, *Angew. Chem. Int. Ed.* 44, 2100 (**2005**).
10. D. W. Wang, H. T. Fang, F. Li, Z. G. Chen, Q. S. Zhong, G. Q. Lu, and H. M. Cheng, *Adv. Funct. Mater.* 18, 3787 (**2008**).
11. S. P. Albu, A. Ghicov, S. Aldabergenova, P. Drechsel, D. LeClere, G. E. Thompson, J. M. Macak, and P. Schmuki, *Adv. Mater.* 20, 4135 (**2008**).
12. L Wang, T. T Zhao, Z Zhang, and G Li, *J. Nanosci. Nanotechnol.* 10, 8312 (**2010**)
13. D. Ma, L. S. Schadler, R. W. Siegel, and J. I. Hong, *Appl. Phys. Lett.* 83, 1839 (**2003**).
14. Y. W. Wang, L. Z. Zhang, K. J. Deng, X. Y. Chen, and Z. G. Zou, *J. Phys. Chem. C* 111, 2709 (**2007**).
15. B. Tan, and Y. Y. Wu, *J. Phys. Chem. B* 110, 15932 (**2006**).
16. J. Y. Lee, J. S. Choi, J. K. Lee, S. K. Choi, and H. D. Chun, *Nanotechnology* 16, 1449 (**2005**).
17. V. V. Kislyuk and O. P. Dimitriev, *J. Nanosci. Nanotechnol.* 8, 131 (**2008**)
18. M. A. Khan, M. S. Akhtar, S. I. Woo, and O. B. Yang *Catal. Commun.* 10, 1 (**2008**).
19. J. Jiu, S. Isoda, F. Wang, and M. Adachi, *J. Phys. Chem. B* 110, 2087 (**2006**).
20. J. Trimboli, M. Mottern, H. Verweij, and P. K. Dutta, *J. Phys. Chem. B* 110, 5647 (**2006**).
21. K. Jiang, X. Hu, H. Sun, D. Wang, X. Jin, Y. Ren, and G. Z. Chen, *Chem. Mater.* 16, 4324 (**2004**).
22. Y. Y. Lin, T. H. Chu, C. W. Chen, and W. F. Su, *Appl. Phys. Lett.* 92, 053312 (**2008**).
23. T. W. Zeng, Y. Y. Lin, H. H. Lo, C. W. Chen, C. H. Chen, S. C. Liou, H. Y. Huang, and W. F. Su, *Nanotechnology* 17, 5387 (**2006**).
24. Q. Wei, K. Hirota, K. Tajima, and K. Hashimoto, *Chem. Mater.* 18, 5080 (**2006**).
25. S. F. Li, G. L. Ye, and G. Q. Chen, *J. Phys. Chem. C* 113, 4031 (**2009**).
26. Z. Zhang, C. C. Wang, R. Zakaria, and J. Y. Ying, *J. Phys. Chem. B* 102, 10871 (**1998**).
27. T. Kasuga, M. Hiramatsu, A. Hoson, T. Sekino, and K. Niihara, *Langmuir* 14, 3160 (**1998**).
28. Q. Chen, W. Zhou, G. Du, and L. M. Peng, *Adv. Mater.* 14, 1208 (**2002**)
29. G. H. Du, Q. Chen, R. C. Che, Z. Y. Yuan, and L. M. Peng, *Appl. Phys. Lett.* 79, 3702 (**2001**).
30. B. D. Yao, Y. F. Chan, X. Y. Zhang, W. F. Zhang, Z. Y. Yang, and N. Wang, *Appl. Phys. Lett.* 82, 281 (**2003**).
31. Z. R. Tian, J. A. Voigt, J. Liu, B. Mckenzie, and H. Xu, *J. Am. Chem. Soc.* 125, 12384 (**2003**).
32. R. Ma, Y. Bando, and T. Sasaki, *J. Phys. Chem. B* 108, 2115 (**2004**).
33. D. R. Zhang, C. W. Kim, and Y. S. Kang, *J. Phys. Chem. C* 114, 8294 (**2010**).
34. D. R. Zhang, Y. H. Kim, and Y. S. Kang, *Curr. Appl. Phys.* 6, 801 (**2006**).
35. J. N. Nian and H. Teng, *J. Phys. Chem. B* 110, 4193 (**2006**).
36. J. D. Donnay and D. Harker, *Amer. Mineral.* 22, 446 (**1937**).
37. R. L. Penn and J. F. Banfield, *Geochim. Cosmochim. Acta* 63, 1549 (**1999**).
38. D. Dvoranova, V. Brezova, M. Mazura, and M. A. Malati, *Appl. Catal. B: Environ.* 37, 91 (**2002**).

39. M. Anpo, T. Shima, S. Kodama, and Y. Kubokawa, *J. Phys. Chem.* 91, 4305 (**1987**).
40. C. Kormann, D. W. Bahnemann, and M. R. Hoffmann, *J. Phys. Chem.* 92, 5196 (**1988**).
41. S. T. Martin, C. L. Morrison, and M. R. Hoffmann, *J. Phys. Chem.* 98, 13695 (**1994**).
42. M. R. Hoffmann, S. T. Martin, W. Choi, and D. Bahnemann, *Chem. Rev.* 95, 69 (**1995**).
43. N. Serpone, D. Lawless, and R. Khairutdinov, *J. Phys. Chem. B* 99, 16646 (**1995**).
44. W. Spengler, R. Kaiser, A. N. Christensen, and G. Müller-Vogt, *Phys. Rev. B* 17, 1095 (**1978**).

Received: 14 July 2010. Accepted: 14 January 2011.